AIAA Propulsion and Energy Forum
10-12 July 2017, Atlanta, GA
53rd AIAA/SAE/ASEE Joint Propulsion Conference

53rd AIAA/ASME/SAE/ASEE Joint Propulsion Conference, 10-12th July, 2017, Atlanta, Georgia.

Combustion Instability and Pressure Oscillation Numerical Simulation in a Solid Rocket Motor

Ainslie D. French, Mario Panelli, Giuseppe Di Lorenzo, Antonio Schettino
CIRA (Italian Aerospace Research Center), Via Maiorise, Capua (CE), Italy 81043

Fabio Paglia
Avio Spa, Corso Garibaldi, 20, - Colleferro (Rome), Italy, 00034

Solid Rocket Motors frequently experience unsteady gas motions and combustion instabilities. Pressure oscillations are a well-known problem of large solid rocket motors (e.g. those of the US Space Shuttle, Arianne 5 P230 and P80). Pressure oscillations lead to thrust oscillations which can generate unstable dynamic environments for the rest of the launcher up to the payload. This kind of instability is governed by the flow behavior of the combusted gas combined with pressure fluctuations and acoustic resonances within the combustion chamber. In the present investigation a computational analysis of the combusted gases passing through the chamber of such a solid rocket motor has been conducted, with particular attention to Corner and Parietal Vortex Shedding instabilities, inside the core section of the motor together with a study of the associated pressure oscillations.

Nomenclature

C_D	=	particle drag coefficient
$D_{s,m}$	=	mass diffusion coefficient for smoke
d	=	diameter, m
E	=	total energy per unit mass, J/kg
F_D	=	drag force, N
h	=	heat of reaction
$\vec{J}_i$	=	diffusion flux, kg/(m^2-s)
κ	=	thermal conductivity, W/(m-K)
L	=	super-droplet loading factor
M_R	=	molecular weight ratio
m	=	mass, kg
$m_{p,0}$	=	original mass of particle at injection, kg
Δm_p	=	change in mass of particle between entrance and exit of cell, kg
$\dot{m}$	=	mass flux rate, kg/m^2 s
$\dot{m}_{p,0}$	=	original mass flux of particle at injection, kg/m^2 s
p	=	pressure, Pa
Re	=	Reynolds number
S	=	source term
T	=	temperature, K

t = time, s
$\vec{u}_p$ = droplet velocity vector, $\vec{u}_p = \{u_{p1}, u_{p2}, u_{p3}\}^T$, m/s
u_r = relative speed between particle and flow, m/s
$\vec{v}$ = velocity vector, $\vec{v} = \{v_1, v_2, v_3\}^T$, m/s
$\vec{x}$ = coordinate vector, $\vec{x} = \{x, y, z\}^T$, m
Y_s = concentration of smoke, kg/m^3
μ = dynamic viscosity, kg/(m-s)
ρ = density, kg/m^3
σ = surface tension of Al_2O_3
$\bar{\bar{\tau}}$ = stress tensor, Pa
ϕ_p = droplet mass composition
χ = mass fraction
ψ = volume fraction
ω = vorticity 1/s

Subscripts and superscripts

bu = burning
$cond$ = condensation
e = energy
ev = evaporation
l = lth droplet
p = droplet
$reac$ = reaction
s = smoke
ρ = density
ρu = momentum

I. Introduction

A typical modern solid rocket motor (SRM) consists of an outer graphite epoxy filament wound casing, a low-density rubber internal insulation, such as polybutadiene and an internal propellant such as hydroxyl-terminated-polybutadiene (HTPB) impregnated with aluminium particles giving rise to a multiphase flow. The nozzle is generally made of a light low cost carbon phenolic material.

During operation the propellant grain regresses over the internal insulation changing both the shape and internal surface area of the combustion chamber. When modelling the combustion process, unsteady calculations are generally performed to capture the changing internal geometry as the propellant steadily combusts. The simulation of this unsteady process can be considered as the modelling of a series of snapshots of the internal chamber geometry at different time intervals.

The goal of the present study is the simulation of the multiphase flow giving rise to pressure oscillations in the axisymmetric geometry of the P80 solid rocket motor at a burn time consistent with the onset of observed pressure oscillations together with a possible explanation of their origin.

The P80 SRM is of particular interest since it is the first stage of VEGA, the new launcher from the European Space Agency, which was qualified with its first two flights from Centre Spatial Guyanais in French Guyana in February 2012 and May 2013. During the SRM development phase, two static firing tests of the P80 were conducted in the

Kourou solid booster test bench in November 2006 and December 2007, providing relevant reference experimental data.

The commercial flow solver ANSYS-FLUENT[1] has been chosen as the pivotal software for the analyses conducted.

This paper is divided into four sections. The first section discusses the physical modelling of the multiphase flow. The second section involves the validation of the numerical method for the compressible Navier Stokes equations using a MILES (Monotone Integrated Large Eddy Simulation) approach combined with a user defined function (UDF) associated with the combustion of aluminium droplets which is applied to the simulation of the ONERA C1 theoretical solid rocket motor, studied by Najjar-et-al[2]. The third section consists of a validation of the present method for non-reacting alumina particles for the C1xb laboratory scale experimental SRM studied by Dupays-et-al[3]. The final part of the paper describes the application of the method to the full scale P80 SRM where pressure oscillations have been observed.

II. Physical Modelling

Modelling of the complex flows inside the combustion chamber of a SRM require sophisticated models to take account of the evolution of the gas mixture, aluminium droplets and aluminium oxide smoke together with all their associated interactions. Since the aluminium droplets are sufficiently large a Lagrangian approach is adopted for their simulation whereas the aluminium oxide particles are sufficiently small to enable an Eulerian approach to be adopted. In the Lagrangian approach there is a finite limit to the number of droplets which can be tracked consequently we consider each computational droplet to be a cluster of droplets associated with a specific number of real droplets.

For the main P80 simulation the present method uses a pressure based algorithm combined with the MILES (Monotone Integrated Large Eddy Simulation) approach to model the time dependent compressible Navier-Stokes equations for mass, momentum and energy. The position, velocity and temperature of the aluminium droplets are calculated via the Lagrangian evolution equations. The present method allows the droplets to be composed of both aluminum (Al) and aluminium oxide (Al_2O_3) representing an oxide cap. The amount of Al_2O_3 in the droplet increases as the droplet passes through and collides with oxide smoke. The droplet suffers a kind of metamorphosis, starting out as being made up of mainly Al but terminating as mainly Al_2O_3.

The droplet combustion is a complex process where initially, once the ambient temperature is higher than the oxide melting point the oxide cap cracks open exposing the liquid Al inside. This liquid Al then vaporizes, advects and diffuses away from the droplet reacting with oxidizers such as O_2, H_2O and CO_2. A reaction front forms around the droplet with the primary product being aluminium oxide. The burning of each droplet is treated in a Lagrangian manner where the burn rate is assumed to be a function of droplet diameter, local temperature and pressure and oxidizer concentration. As the droplets collide and agglomerate with the oxide smoke particles the oxide caps of the aluminium droplets grow. The collision process is driven by the relative velocity between the droplet and the surrounding smoke particles.

As a consequence of the combustion process the aluminium droplets impinge on the mass, momentum and energy of both the gas mixture and the oxide smoke field giving rise to a coupling between the Lagrangian droplet and the gas mixture on which it is carried. If the number of droplets per cell is significantly high then the Eulerian field which influences the mixture and evolution of the smoke will remain acceptably smooth, and will be fairly representative of the real effect of the Lagrangian droplet field on the gas mixture.

If very fine particles are assumed then the smoke concentration field can be modelled using the modified density approach. In this approach it is assumed that the smoke advects at the same velocity as the surrounding gas and consequently only the field associated with smoke concentration requires to be evolved as a scalar field. The main advantage of this approach is that the solution of the additional momentum equations for the smoke phase is avoided.

Thus, in addition to the usual model for the solution of the transport equations, based on Navier-Stokes equations, with or without a turbulence model (Eulerian phase), the proposed approach requires five additional mechanisms,

which represent the different phenomena involved and have been coded into an appropriate FLUENT user defined function (UDF).

These mechanisms are: the Lagrangian model for large particles (agglomerate); the Aluminum combustion model; Coupling between agglomerates and gas (Lagrangian-Eulerian coupling); Coupling between agglomerates and Al_2O_3 smoke and the Break-up model.

and are discussed in Sections II.A to II.G

A. Numerical Solution of the Transport Equations

The flow field is simulated using FLUENT 15.0 which is a general purpose commercial code for fluid dynamics simulations created by Fluent Inc. Regarding turbulence modelling, the first test case assumes laminar flow whereas for the second test case and main P80 simulation the MILES approach is adopted. The relevant transport equations are discretized in space with the Finite Volume approach, using the density based algorithm for the first test case and a pressure based algorithm for the second test case. Unsteady calculations are performed in all simulations where a fixed time stepping method is implemented.

B. The MILES approach

The Large Eddy Simulation (LES) approach is based upon the hypothesis that the turbulent field can be separated by the application of a spatial filter, in the large, energy-containing eddies, to be explicitly resolved using a time-marching calculation, and the small-scale eddies, to be modelled using an adequate sub-grid stress model (SGS). An alternative approach is to use an implicit SGS as proposed by Boris-et-al[4] with the monotonically integrated LES (MILES) concept.

This approach relies upon the fact that any high-order upwind scheme coupled to a non-linear limiter generates a numerical dissipation of order $O(\Delta^2)$, which is proportional to the grid size (Δ) and thus proportional to the spatial filter applied in the LES approach. Consequently, this numerical term is similar to the explicit sub-grid diffusivity of classical SGS and could replace it.

The second test case and P80 simulation use the MILES approach applying the PISO (Pressure Implicit with Splitting of Operators) algorithm using central differencing for the momentum fluxes of the convection term while the pressure in the momentum equation is calculated to second order via the Skewness-Neighbour-Coupling between velocity and pressure.

C. Lagrangian Model for large Particles

The complex mechanism of aluminum combustion in a solid propellant may be described as follows. During the burning of the solid propellant Al particles emerge at the surface when the propellant burns. Typically two sets of different particles, large agglomerates (size ≈100μm) and non-agglomerate small particles (size≈30μm), leave the propellant surface as shown in Figure 1.

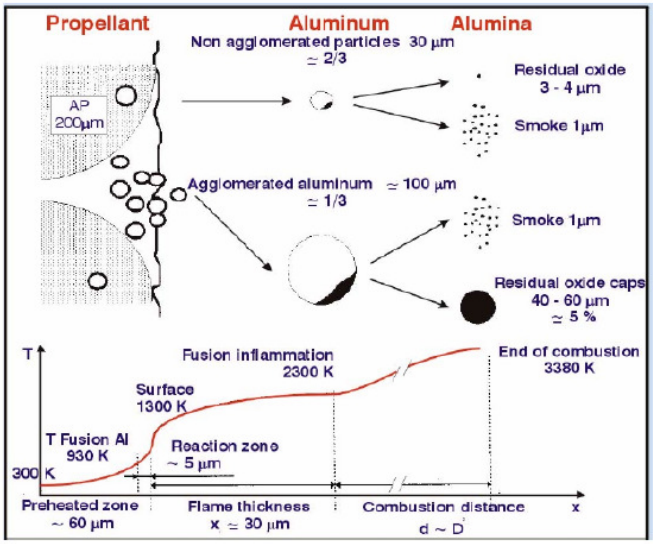

Figure 1 : Al particle injection phases

The non-agglomerated particles (which represent about 2/3 of the Al mass) escape individually from the surface, producing, as a product of combustion, mainly 1 µm smoke (Al_2O_3). The agglomerated particles produce as final products, both particles having residual oxide caps (Al_2O_3) with a size of a few tens µm (≈40-60mm) as well as participating in the production of Al_2O_3 smoke having a size of ≈1µm.

The end of the combustion occurs only when either the Al has been totally consumed, or more often when the alumina accumulation has so deeply incorporated the remaining part of the Al that the surface on which the reaction can occur is negligible. Beckstead[6] estimates the burn time as the time required for 95% of the particle to be consumed.

The agglomerated particles (which are about 1/3 of the original Al mass) have a not-negligible life time and burn away from surface. Therefore, they require an explicit treatment during their transport through the combustion chamber (Lagrangian Approach).

The Lagrangian evolution equations for the droplet position vector χ_p, velocity vector u_p are:

$$\frac{d\vec{x}_p}{dt} = \vec{u}_p, \qquad \frac{d\vec{u}_p}{dt} = F_D\left(\vec{v}\left(x_p\right) - \vec{u}_p\right),$$

with

$$F_D = \frac{18\mu}{\rho_p d_p^2}\frac{C_D \,\mathrm{Re}}{24}, \qquad C_D = \frac{24\left(1 + 0.15\,\mathrm{Re}^{0.687}\right)}{\mathrm{Re}} \tag{1}$$

where ρ_p and d_p are the droplet density and diameter respectively.

The remaining non agglomerated particles (which represent about 2/3 of the Al mass) escape individually from the surface, these particles have a short life time and burn near the surface. They produce mainly 1 µm smoke as the product of combustion.

The smoke particles of alumina are very small and their number is enormous and consequently they cannot be treated in a Lagrangian manner, therefore they are described with an Eulerian approach.

In the present model gaseous combustion products from propellant and smoke particles are considered as a unique gas mixture and the gas properties are modified to account for the presence of smoke.

D. Aluminium Combustion Model

The combustion of an Al droplet is a complex process. Once the ambient temperature exceeds the oxide melting point, the oxide shell around the droplet cracks and exposes the liquid Al. Aluminum vaporizes, advects, and diffuses away from the droplet and reacts with the oxidizers (such as O2, H2O, CO2) which are present. A reaction front forms around the droplet where the primary product of combustion is aluminum oxide.

Although the reaction takes place in the gas phase, considering the scale of the rocket, it is not possible to resolve the gas phase chemistry that occurs around each droplet. Thus the burning of each droplet is treated in a Lagrangian manner. The burn rate of a droplet is assumed to follow a general power-law relation dependent on the droplet diameter, local pressure and temperature, and oxidizer concentration.

The correlation proposed by Widener and Beckstead[7] as the model for the Al droplet burn rate is used here:

$$\dot{m} = c\rho_{Al} T^{1.57}\left(x_p\right) p^{0.2}\left(x_p\right) \chi_{eff}^{0.39} D_{rel} d_p^{1.1} \psi_{Al} \tag{2}$$

where the constant of proportionality $c = 2.885\times10^{-13}$ in SI units, whereas the effective oxidizer mass fraction χ_{eff}, is defined in terms of individual components as:

$$\chi_{eff} = \chi_{o_2} + 0.58\chi_{H_2O} + 0.22\chi_{CO_2} \tag{3}$$

When different oxide components cannot be individually isolated and traced then χ_{eff} may be calculated based on conditions of the core flow in the rocket chamber and D_{rel} is defined as:

$$D_{rel} = 1 + 1.27\chi_{H_2} \tag{4}$$

The burn rate model does not account for the fact that part of the droplet is made up of an oxide cap. To include the presence of the oxide cap the burn rate model is scaled with the volume fraction of aluminium as:

$$\psi_{Al} = \frac{\phi_{Al}\rho_{Al_2O_3}}{\Phi_{Al}\rho_{Al_2O_3} + \left(1-\Phi_{Al}\right)\rho_{Al}} \tag{5}$$

where the mass fraction of aluminium within the droplet, Φ_{Al}, is defined as:

$$\Phi_{Al} = \frac{m_{Al}}{\left(m_{Al} + m_{Al_2O_3}\right)} \tag{6}$$

E. Coupling between Agglomerate and Gas (Lagrangian-Eulerian Coupling)

As a consequence of the burning process, the aluminium droplets influence the mass, momentum and energy of both the gas mixture and the oxide smoke field. As a result there is a coupling of the Lagrangian droplet onto the gas mixture which is carrying the droplet.

As long as the number of droplets per cell is significant, the resulting Eulerian field which influences the evolution of the smoke and mixture will be sufficiently smooth and will closely resemble the true influence of the Lagrangian droplet field on the gas mixture.

Assuming that during the burning process the following stoichiometric relation holds:

$$2Al(l)+3O(g)\rightarrow \alpha Al_2O_3(s)+(1-\alpha)Al_2O_3(g) \tag{7}$$

where α is the fraction of alumina which condenses to the solid state as smoke particles.

The continuity equation and mass source for the gas mixture are:

$$\frac{\partial \rho}{\partial t}+\nabla\cdot(\rho\vec{v})=S^p_{\rho,l}, \quad S^p_{\rho,l}=\frac{\Delta m_p}{m_{p,0}}\dot{m}_{p,0} \tag{8}$$

where $m_{p,0}$ is the original mass of the particle at injection, $\dot{m}_{p,0}$ is the original mass flux of the particle at injection and Δm_p is the change in mass of the particle between when it enters and exits the cell.

The momentum equation and momentum source for the gas mixture are:

$$\frac{\partial(\rho\vec{v})}{\partial t}+\nabla\cdot(\rho\vec{v}\vec{v})=-\nabla p+\nabla\cdot(\bar{\tau})+S_{\rho\vec{v},l}, \; S_{\rho\vec{v},l}=\sum\left(\frac{18\mu C_D\,\mathrm{Re}}{\rho_p d_p^2 24}(\vec{u}_p-\vec{v}(x_p))\right)\dot{m}_p\Delta t \tag{9}$$

and

$$\bar{\bar{\tau}}=\mu\left[(\nabla\vec{v}+\nabla\vec{v}^T)-\frac{2}{3}\nabla\cdot\vec{v}I\right], \quad C_D=\frac{24(1+0.15\,\mathrm{Re}^{0.687})}{\mathrm{Re}} \tag{10}$$

The energy equation and energy source for the gas mixture are:

$$\frac{\partial(\rho E)}{\partial t}+\nabla\cdot(\vec{v}(\rho E+p))=\nabla\cdot(\kappa\nabla T+(\bar{\bar{\tau}}\cdot\vec{v}))+S^p_{e,l}, \qquad S^p_{e,l}=L\dot{m}_{bu,l}h_b+L\dot{m}_{cond,l}h_{cond} \tag{11}$$

where L represents the ratio of the number of real to computational droplets, $\dot{m}_{by,l}$ is the rate at which the aluminium of the lth droplet burns, $\dot{m}_{cond,l}$ is the rate at which the oxide condenses and the effective heat of release h_b of the combustion process is:

$$h_b=-h_{ev}+h_{reac} \tag{12}$$

F. Coupling between Agglomerates and Al_2O_3 Smoke

The species transport equation and source term for the gas mixture are:

$$\frac{\partial((\rho Y_s))}{\partial t}+\nabla\cdot(\rho\vec{v}Y_s)=-\nabla\cdot\vec{J}_s+S_s, \qquad S_s=\eta_{Al_2O_3}\dot{m}_{bu}L \tag{13}$$

with

$$J_s = -\rho D_{s,m} \nabla Y_s, \qquad \eta_{Al_2O_3} = \%\ Al_2O_3\ smoke \tag{14}$$

The chemical reaction process is considered to be fully completed and so there are no contributions to the source term from volumetric reactions. Additionally contributions to diffusion, $\vec{J}_i$, from thermal diffusion are also ignored.

One of the products of Al combustion is the oxide smoke which is made up of very fine Al_2O_3 particles being about 1μm in size. This smoke is treated using an Eulerian approach. Consequently, in the continuum equations each droplet acts as a local source of oxide smoke particles.

G. Break up Model

When an initially spherical drop encounters an ambient flow field moving at a velocity relative to it, if the air velocity is high enough, aerodynamic force causes the drop to deform and break apart into fragments. This process is referred to as secondary atomization or secondary breakup, which plays an important role in the increase of surface area and the enhancement of heat and mass transfer between the fuel and the ambient gas.

In the secondary atomization of a Newtonian liquid, the Weber number (We) and Ohnesorge number (Oh) are the two most important parameters. The Weber number represents the ratio of disruptive aerodynamic force to the stabilizing surface tension force,

$$We = \frac{\rho_g u_r^2 D_0}{\sigma} \tag{15}$$

where ρ_g is the gas density, u_r is the relative speed between the particle and the flow, D_0 is the particle diameter and σ is the surface tension of aluminium oxide.

Different ranges of We are associated with different forms of break-up. At the lowest range of We number (We < 12) vibrational break-up occurs. This kind of break up is based on a steady amplification of the droplet deformation and is excluded from the current model since the characteristic time for this kind of break-up is very large compared with the residence time of aluminium particles in the combustion chamber of a SRM.

The most appropriate form of break-up for the SRM scenario is the second category “bag break-up” which occurs in the range of We numbers (12 < We < 50). Preliminary analyses of existing data and SRM flow fields indicate that this range of We number occurs frequently with current distributions of Aluminium particles in SRM flow fields.

Experimental results from Zhao[8] show that the fragment distribution of ring and stamen can be described by log-normal or gamma distributions, which are common in the study of atomization fragmentation.

The Sauter mean diameter (SMD) is one of the most widely used mean drop size in atomization. SMD can be defined as the diameter of a drop having the same volume/surface area ratio as the spray. SMD is especially important in liquid atomization and combustion. The SMD of the fragmented particles is equal to 0.31 of the initial drop diameter.

Hence, for the sake of simplicity and efficiency in the present model, after breakup, the diameter of the finer particles are assumed to be 1/3 of the diameter of the original droplets.

III. Validation

Fundamental to the Lagrangian representation of aluminium droplets in SRM calculations is the method of injection of the particles from the propellant surface into the combustion chamber. In the present work four cases have been simulated which have different initial droplet distributions. For the ONERA C1 calculations two skewed logarithmic distributions (SLDA, SLDB), and one normal logarithmic distribution (LND), see Table 1, have been used. For the C1xb calculation a constant distribution of 6µm particles has been used and for the P80 target test case of interest, the same normal logarithmic droplet distribution as the ONERA C1 has been used.

Table 1 : Particle Distributions

	Min (µm)	Peak (µm)	Max (µm)	Standard Deviation
SLDA	5	30	240	1.3
SLDB	5	30	190	1.0
LND	-	30	-	0.25

ONERA –C1

The first validation test case, the ONERA-C1 configuration described by Najjar-et-al[2] is shown in Figure 2. This test case is a two-dimensional planar version of the ONERA C1 axisymmetric configuration investigated by Najjar-et-al[2] and originally proposed by Lupoglazoff-et-al[5] as both planar and axisymmetric configurations. In the present method the central axis uses the symmetry plane rather than the axisymmetric boundary condition. A fully structured grid of 810 x 80 cells has been used with associated stretching in the tapered regions. The upstream taper location is important since this is the origin of vortex shedding. Comparison of the temperature and vorticity contour plots with those obtained by Najjar for the skewed logarthimic distribution SLDB show good agreement, see Figure 3 and Figure 4.

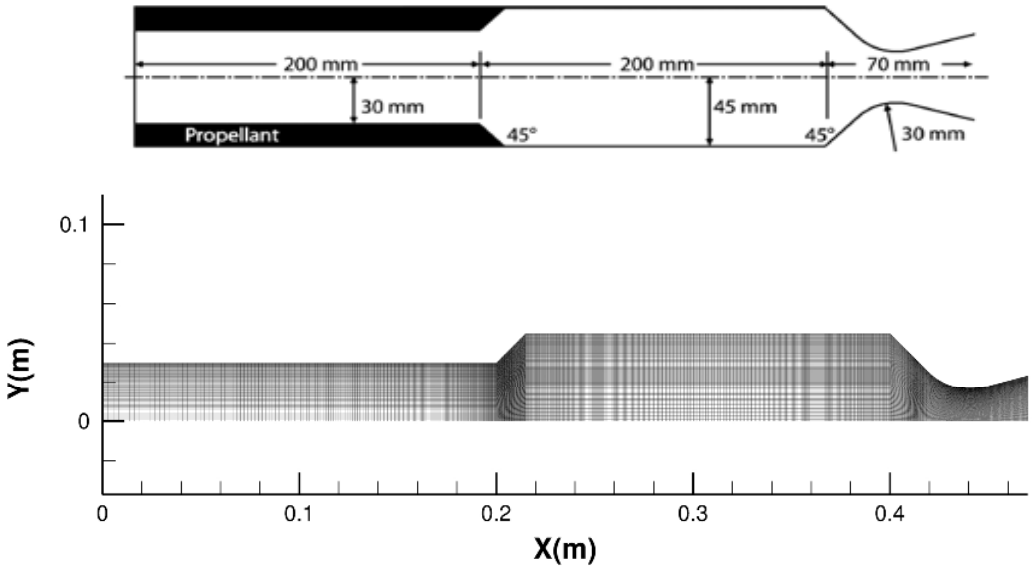

Figure 2 : C1 – Geometry and Grid

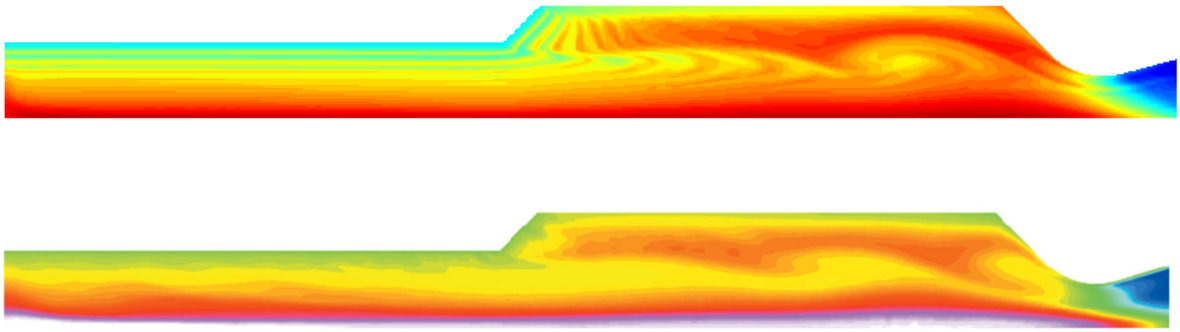

Figure 3 : SLDB : Comparison of C1 Temperature Distributions Present Work (top) – Najjar (bottom)

(T_{min} = 3000K, T_{max} = 4000K, ΔT = 20K)

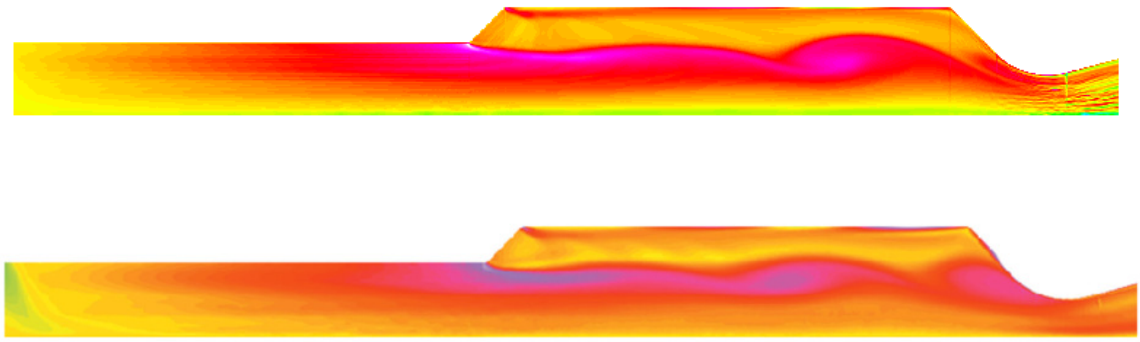

Figure 4 : SLDB : Comparison of C1 Vorticity Distributions Present Work (top) – Najjar (bottom)

(ω_{min} = -5x10^{4}s^{-1}, ω_{max} = 5x10^{4}s^{-1}, $\Delta\omega$ = 10^{3}s^{-1})

Figure 5 shows a comparison of results between the present method and Najjar for particle velocity, mean diameter and aluminium mass fraction profiles at the beginning of the nozzle inlet for the three distributions, SLDA, SLDB and LND. There is fairly good quantitative agreement between both sets of results.

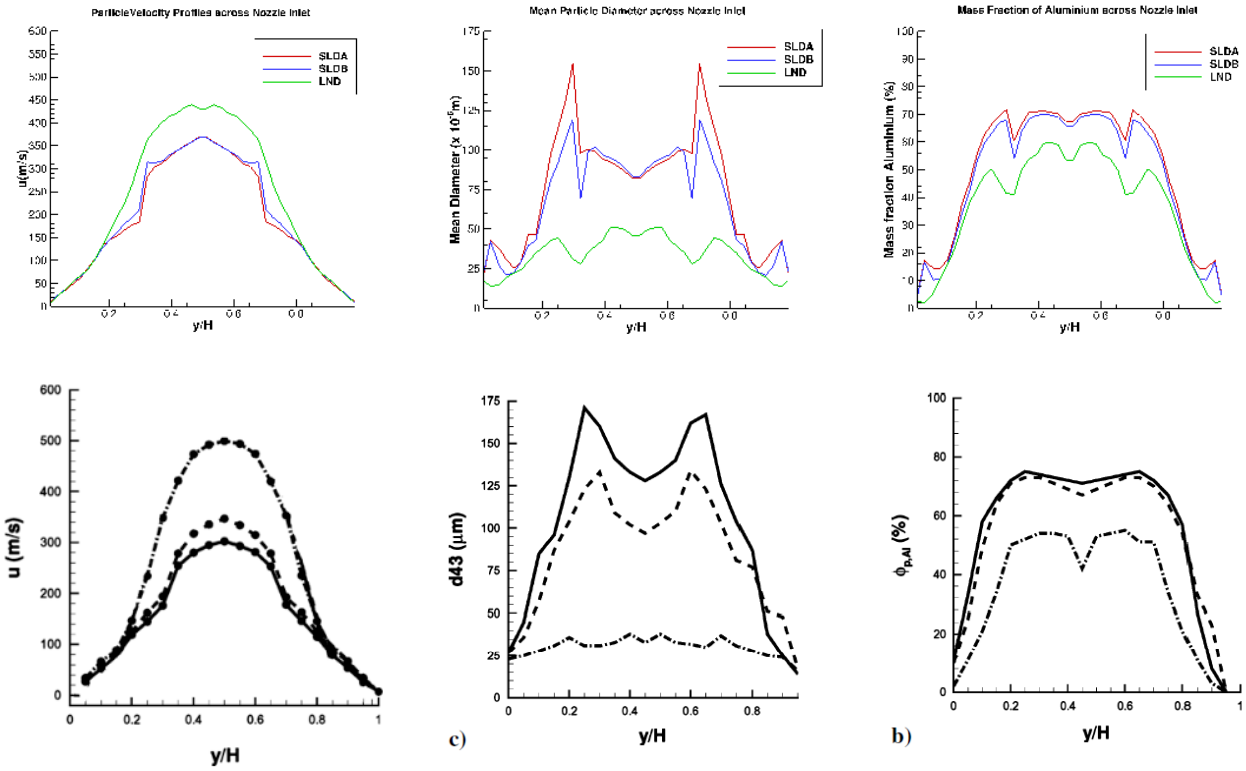

Figure 5 : Comparison of C1 Particle Velocity, Mean Diameter and Aluminium Mass Fraction distributions across nozzle inlet - Present Work (top) – Najjar (bottom)

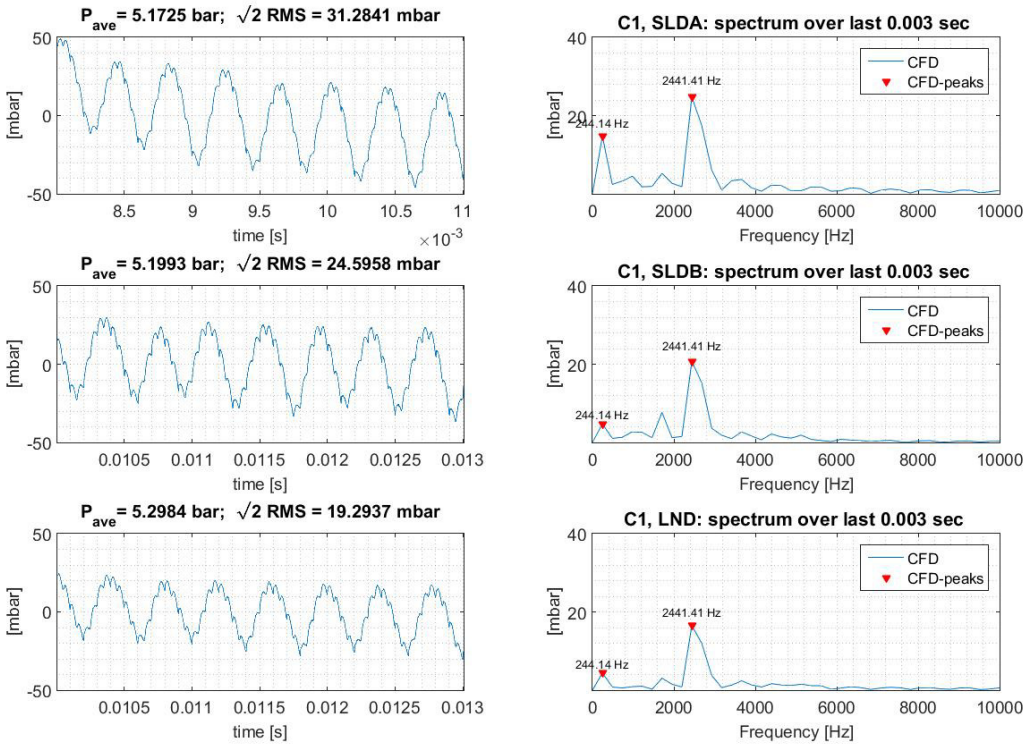

Figure 6 : Comparison of C1 Pressure Oscillations at chamber head for SLDA, SLDB and LND particle distributions

Figure 6 shows a comparison of pressure distributions for the C1 test case. These were not reported by Najjar but show fairly consistent results where the largest amplitude pressure amplitude oscillations occurring for the SLDA distribution, followed by the SLDB distribution and the LND distribution having the smallest amplitude oscillations.

C1xb

The second validation test case is the C1xb experimental laboratory scale SRM cited by Dupays-et-al[3].and shown in Figure 7 below.

This validation test case is divided into two simulations, the first is associated with a simulation without particles and the second is associated with a simulation consisting of a regular distribution of 6 µm non combusting aluminium oxide particles. In both cases the configuration corresponds to 3mm of web thickness burned.

Axisymmetric calculations have been conducted for both simulations using the both a 507x41 point grid, a 597x49 point grid and a 1083x81 point grid. The 597x 49 point grid is shown in Figure 8.

Figure 9 show results for pressure oscillations both at the fore and aft ends of the combustion chamber in the vicinity of the throat and Figure 10 shows a comparison of amplitudes of pressure oscillations along the combustion chamber for different grids compared with numerical and experimental results cited by Kourta[9]. Whilst all calculations overestimate the amplitude of pressure oscillations, the results from the present method appear closest to experimental results on the finest grid

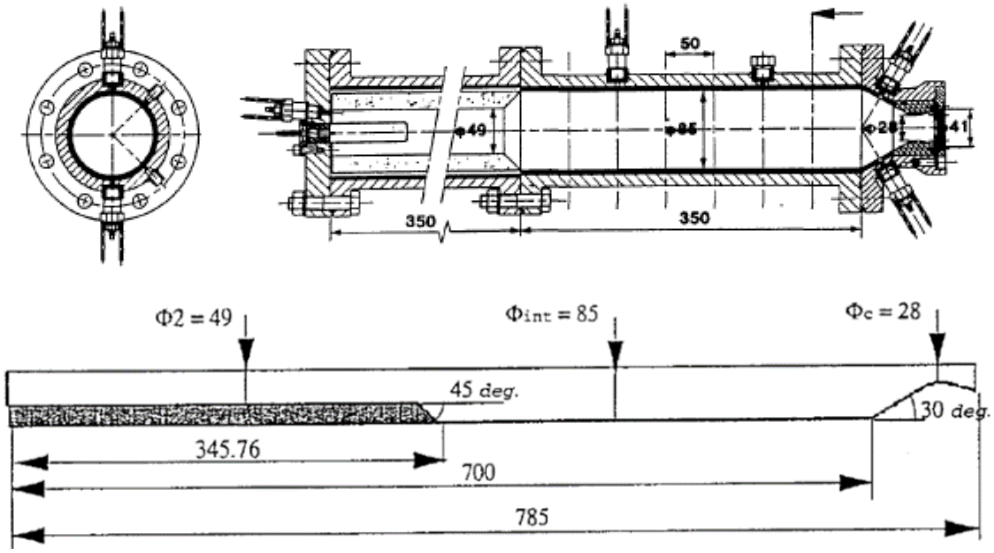

Figure 7 : Experimental Set up and Geometry of test case C1xb

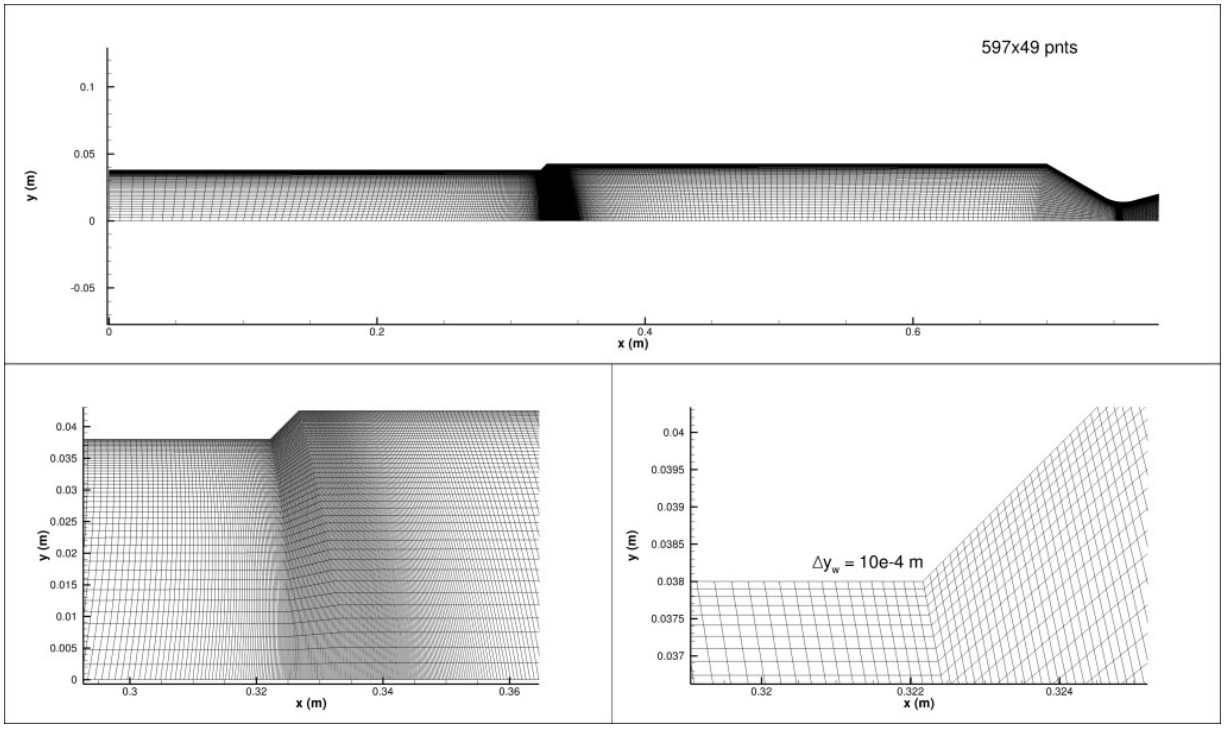

Figure 8 : C1xb - Grid details

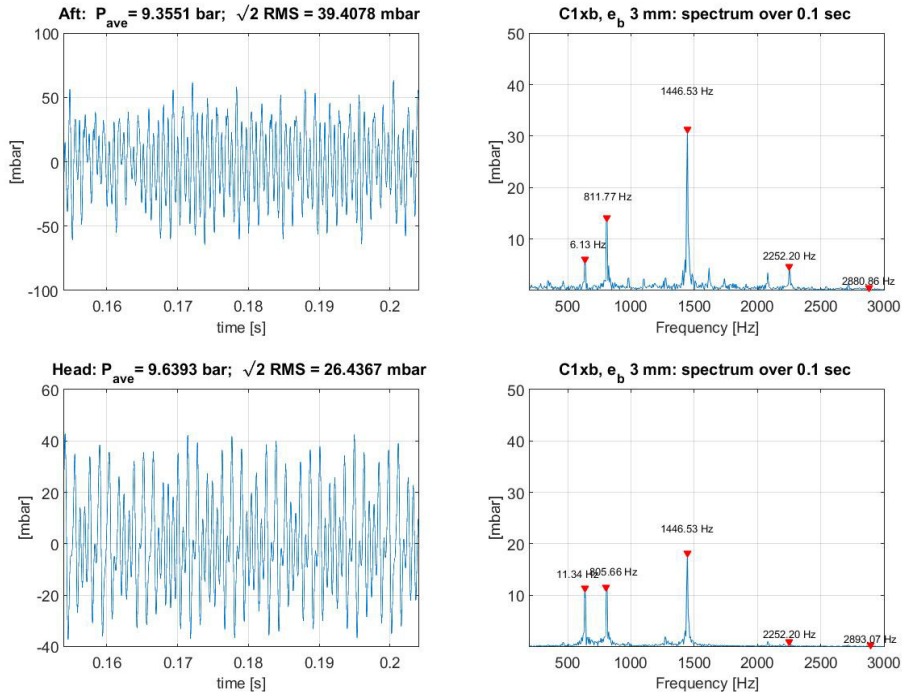

Figure 9 : C1xb – Pressure Oscillations on 597 X 49 point grid without particles

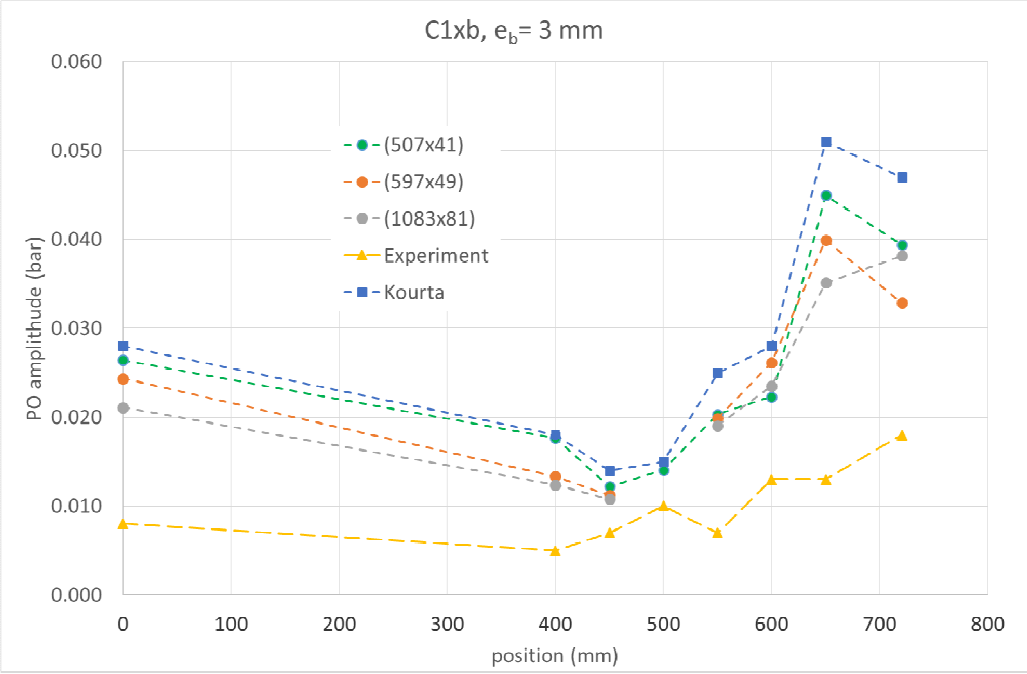

Figure 10 : C1xb without particles – Comparison with numerical and experimental data (Kourta[9])

Figure 11 and Figure 12 show results for the C1xb configuration with the injection of 6µm particles of aluminium oxide. Figure 11 indicates not only the presence of vortices originating from the corner of the upstream taper but also the particle distribution and residence time associated with different regions of particles in the chamber.

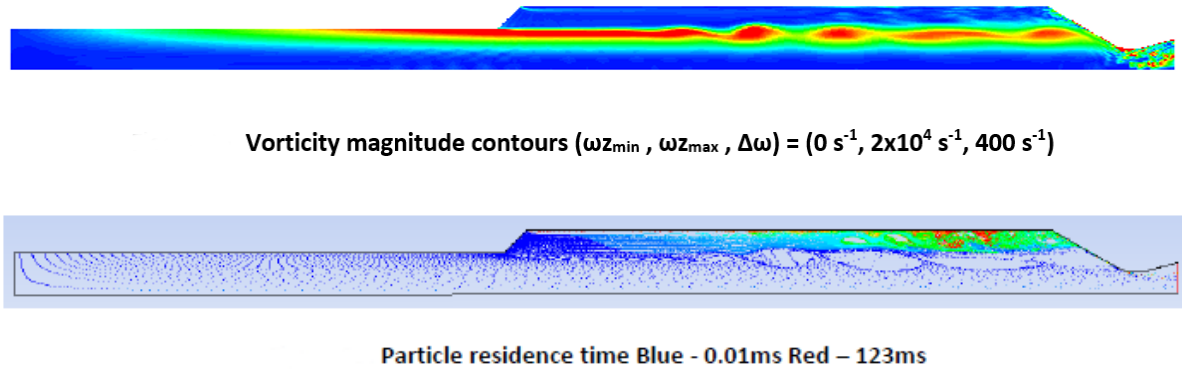

Figure 11 : C1xb with 6 µm particles – Vorticity Magnitude and Particle Residence Time

Figure 12 shows the root mean square values of pressure at various locations along the chamber wall compared with experiment for cases both with and without particles. There is very good agreement between the present numerical method and experimental results.

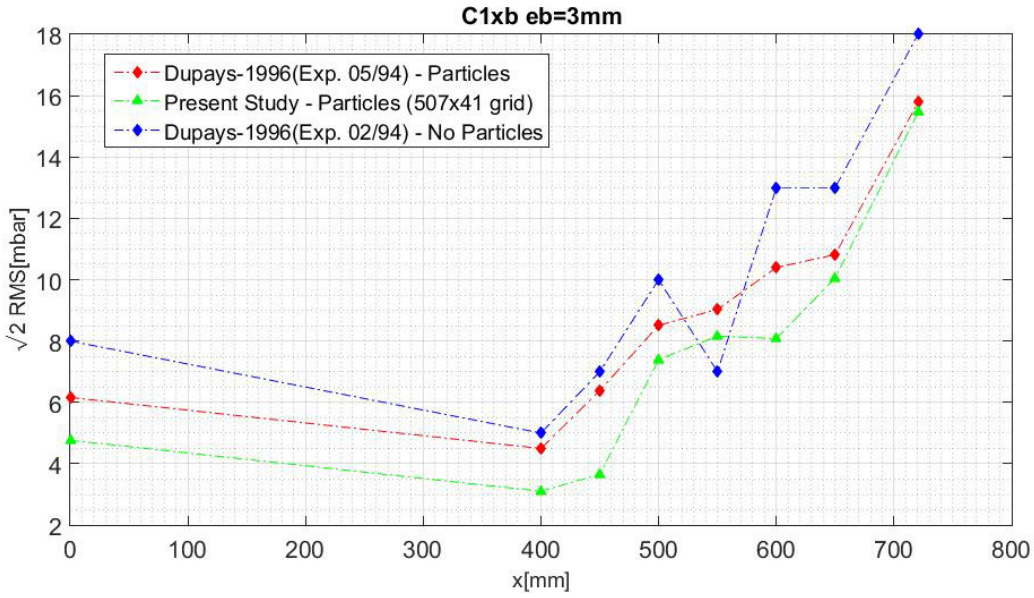

Figure 12 : C1xb - Comparison with of present numerical method with experimental data

IV. P80 SRM - Results and Discussion

The method has then been applied to the target case of interest, the P80 SRM. The SRM combustion chamber geometry and the experimental pressure oscillation data have been provided by AVIO spa. A sensitivity analysis

associated with the grid sizes has been conducted to verify the capability of the model to reproduce the experimental results.

A. No Particles

A grid sensitivity analysis was conducted for hydrodynamic simulations (single phase without particles) to obtain an optimized grid which was sufficiently well-defined and relatively light weight to enable efficient two-phase flow calculations to be performed. Grid suitability was judged on the ability of the computation to reproduce the target frequency and amplitude of the first acoustic mode of the P80 combustion chamber associated with two static firing tests (P80 DM and P80 QM) and two VEGA flights (VV01 and VV02).

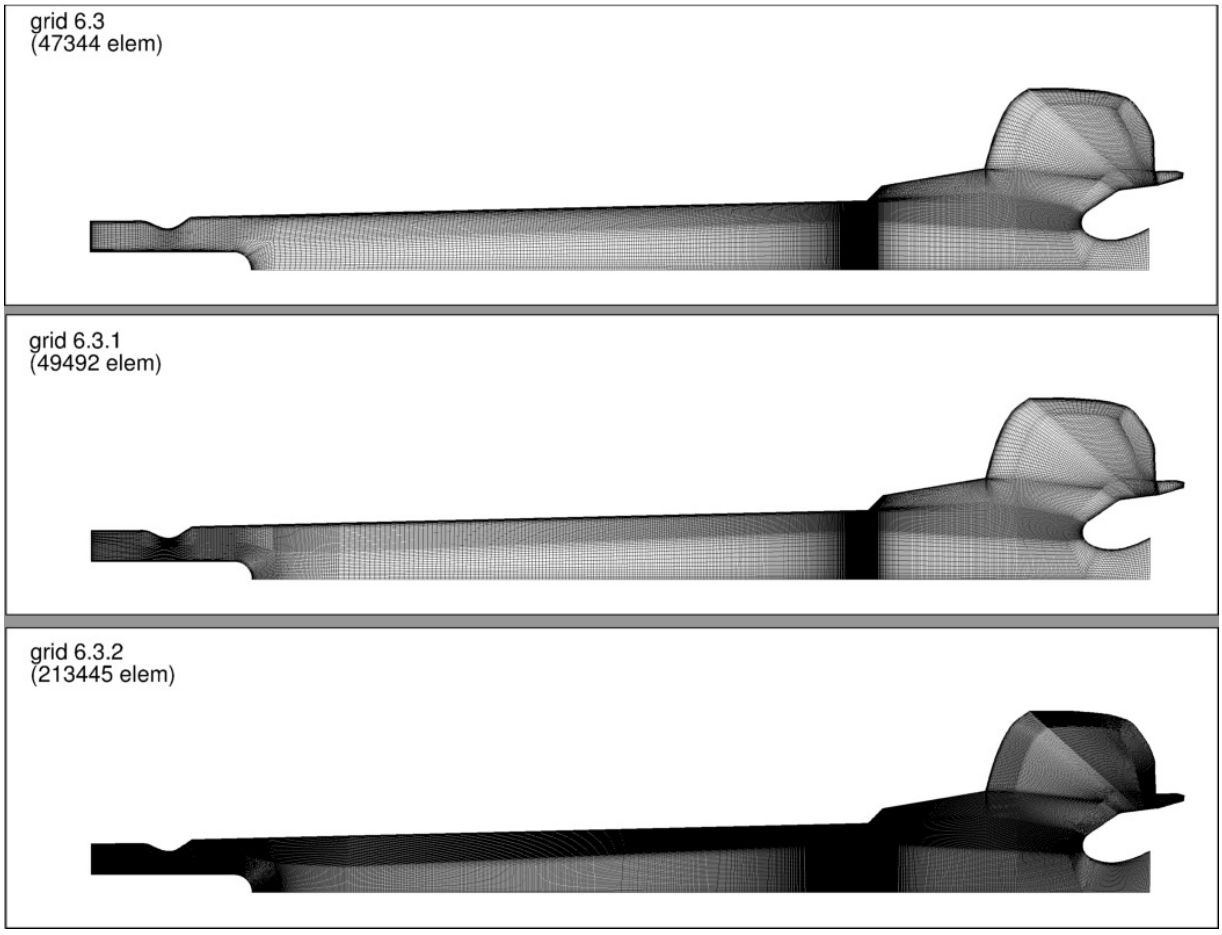

Figure 13 : P80 – Grids used for hydrodynamic sensitivity study.

Figure 13 shows three grids which produced results within the proximity of the experimental data and consequently were considered suitable for the study of flow characteristics and pressure oscillations for the hydrodynamic test case.

The vorticity distributions for this hydrodynamic test case on each of the above grids are shown in Figure 14.

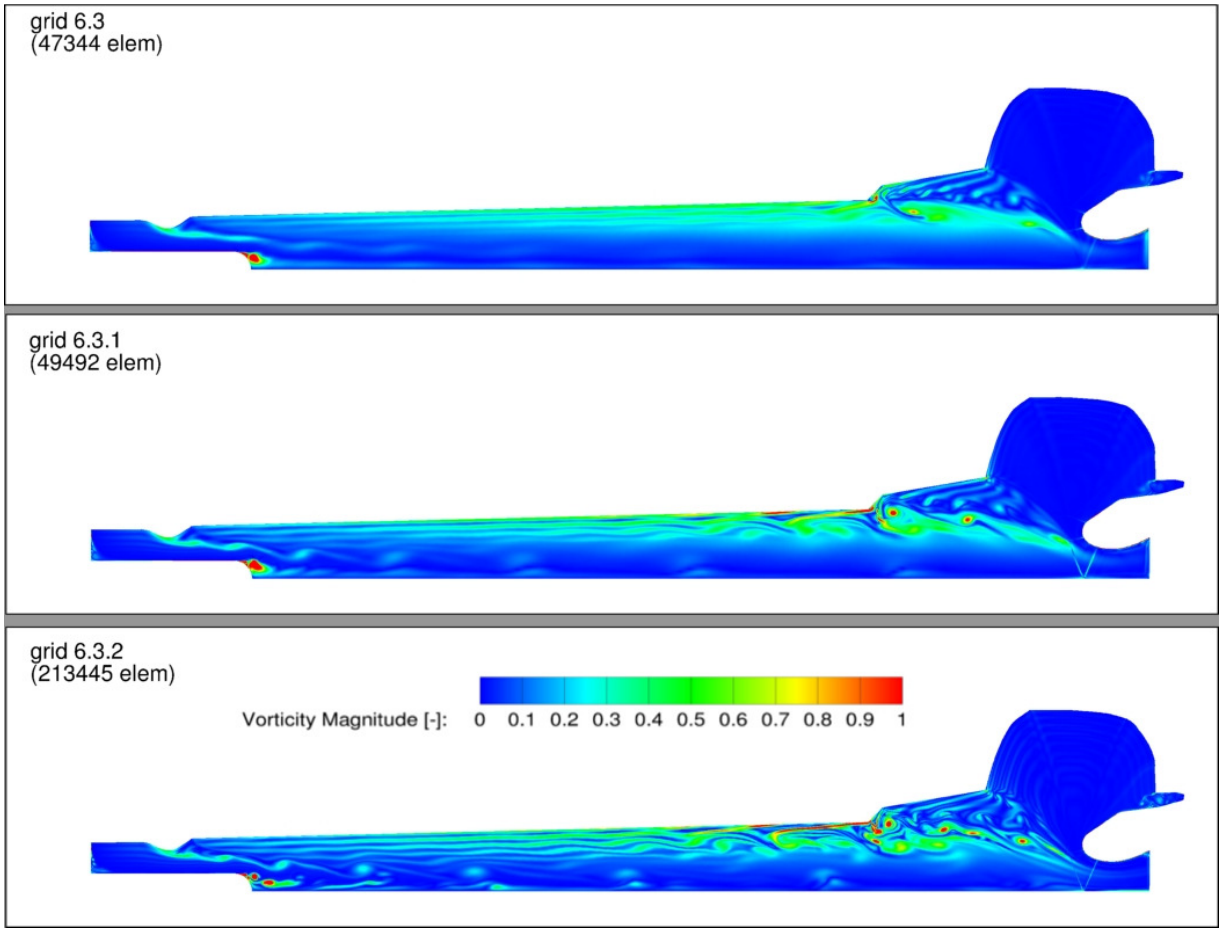

Figure 14 : P80 – Vorticity distributions on grids used for hydrodynamic sensitivity study.

The vorticity details are best resolved on the finest grid, grid v6.3.2. Vorticity is generated from four regions: parietal vortex shedding (PVS) from the cylindrical grain surface, corner vortex shedding (CVS) from the cylindrical-star grain junction, from the bump above the igniter and also from the downstream upper end of the igniter.

In these simulations, following the ideas of Gallier-et-al[11] the large aft cavity, due to the presence of the submerged nozzle, may be responsible for part of the instabilities in the hydrodynamic calculation. According to Anthoine[12,13] an aft-cavity can produce significant acoustic power. His reasoning was based on the Howe[14] acoustic analogy and showed that the acoustic power produced is proportional to

$$\iiint_V (\omega \cdot \bar{v}).u' dV$$

where ω, $\bar{v}$ and u' are the vorticity, mean velocity and acoustic velocity vectors respectively. When a vortex traverses the front of the entrance to the cavity the acoustic velocity vector, u', is almost normal to the vortex path and creates sound.

Figure 15 shows the convergence histories of chamber pressure for each of the three grids studied. It should be noted the presence of "beats" associated with grids 6.3 and 6.3.1 which are not present for grid 6.3.2 and so it is concluded that these are grid related. However, it should be noted that for grid 6.3.1 the beats disappear after a brief interval. The same average chamber pressure is achieved in each case.

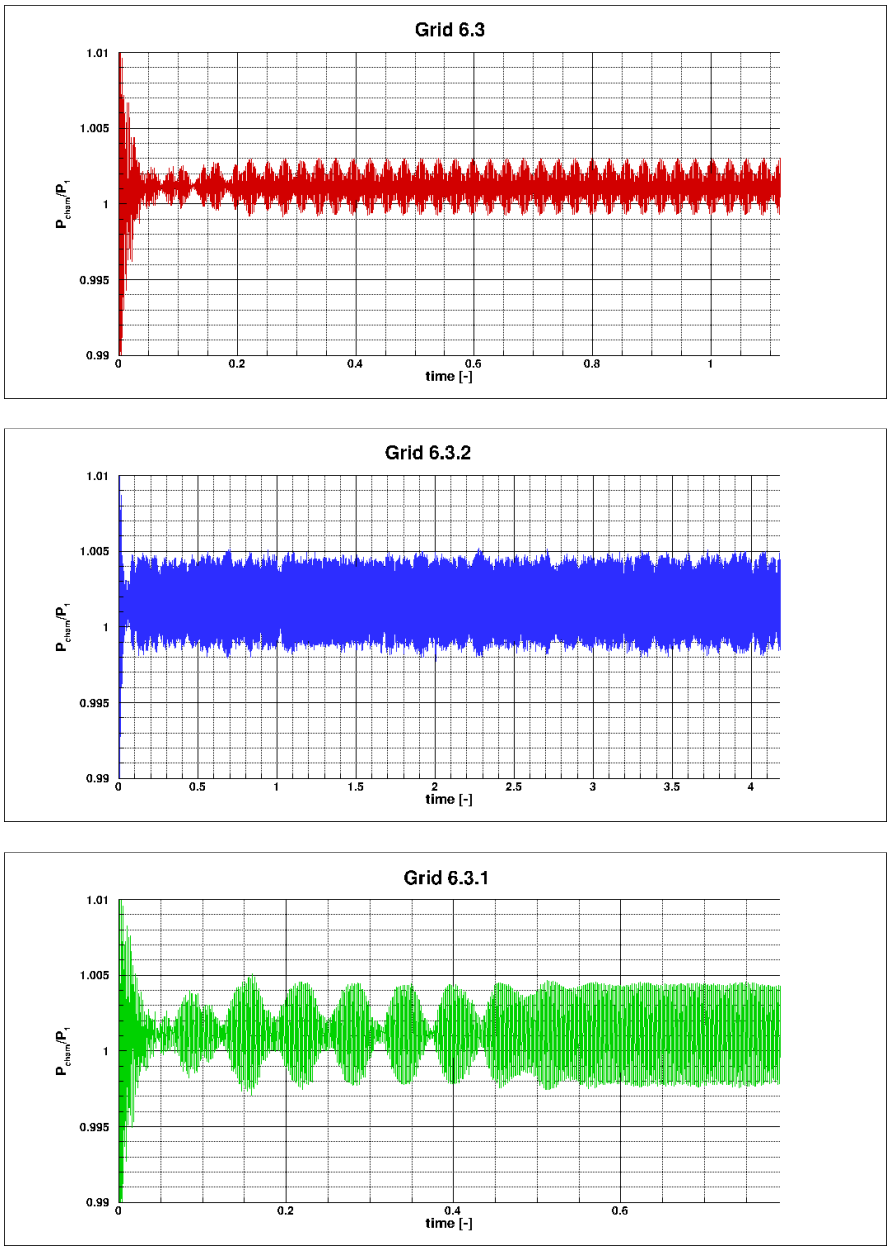

Figure 15 : P80 - Convergence histories of chamber pressure on different grids.

Fourier Analyses of pressure oscillations showing details of frequencies and amplitudes for each of the three grids are shown in Figure 16. The computed instability frequency closely matches the measured frequency for all grids but the amplitudes calculated on grid 6.3 fall below the experimental range whereas the amplitudes on grid 6.3.1 slightly overestimate the maximum experimental value, however, those of grid 6.3.2 are within the range of the experimental values.

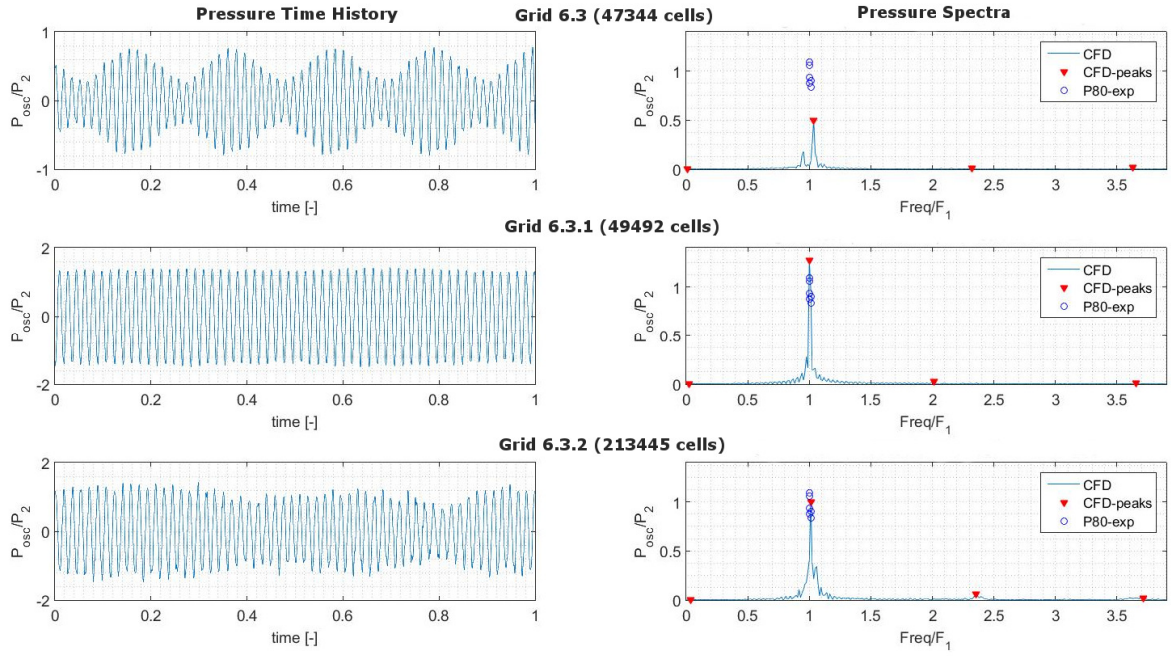

Figure 16 : P80 - Fourier Analysis of chamber hydrodynamic pressure oscillations for each of the three grids

These results for the hydrodynamic case show that when using a customized finer grid in the region of the igniter (grid 6.3.1 vs. grid 6.3), the same regular level of oscillations are obtained as those present on the finest grid (grid 6.3.2) where the low frequency oscillation is eliminated.

Four sources of vortex shedding are present, three associated with CVS locations and one associated with PVS.

There is good agreement with experiment for the computed instability frequency on all grids whereas the amplitudes tend either to underestimate or slightly overestimate experimental values on the coarser grids. Only the amplitudes on the finest grid are in best agreement with experiment. It is hypothesized that the large aft cavity may be responsible for a significant contribution to the instabilities due the generation of sound waves as the vortices travel almost normally across the cavity entrance.

For reasons of expediency grid v6.3.1 was used for the subsequent calculations. Compared to experimental results the amplitude of the oscillations on this grid is larger. A reduction in the amplitude of the oscillations is expected in the presence of particles.

B. With Particles

In the following a comparison of inert and combusting particles on grid 6.3.1 is presented where the LND particle distribution is used in both cases. The same total mass flux is used as in the hydrodynamic case, the only difference being that HTPB binder is impregnated with 19% Al particles.

Figure 17 shows the effect on vorticity of particle combustion compared to inert particles. Both flows have the same injection and particle mass fluxes.

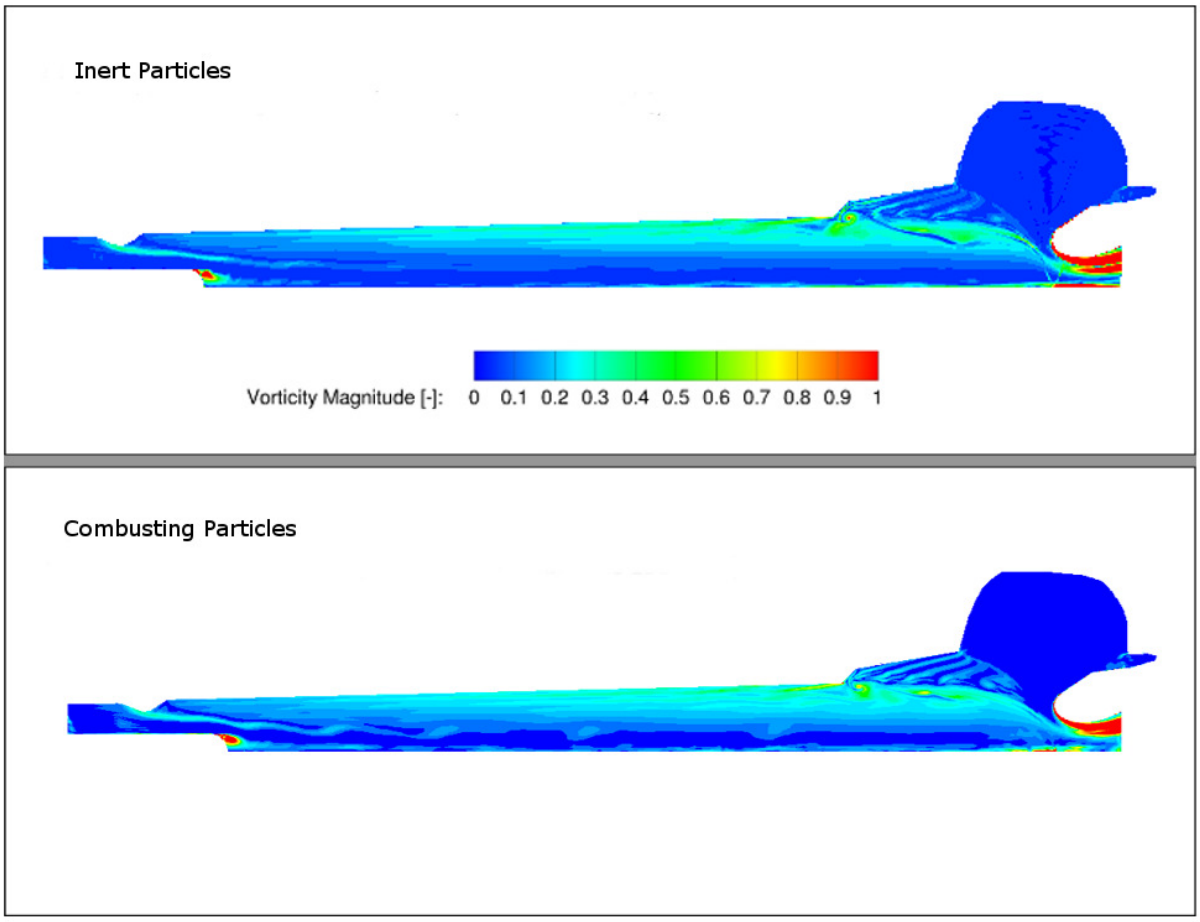

Figure 17 : P80 - Effect on vorticity distribution for same mass flux ; inert (top) , combusting particles (bottom)

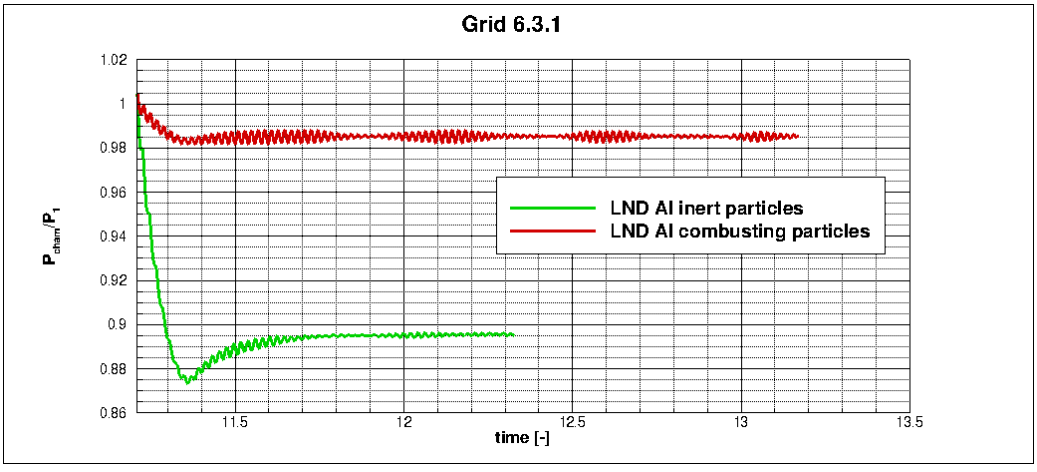

Figure 18 : P80 - Effect of particle combustion on chamber pressure

Figure 18 below shows the convergence histories of chamber pressure for the inert and combusting particle calculations. The chamber pressure rises by almost 11% and the amplitude of the pressure oscillations is also greater for combusting particles.

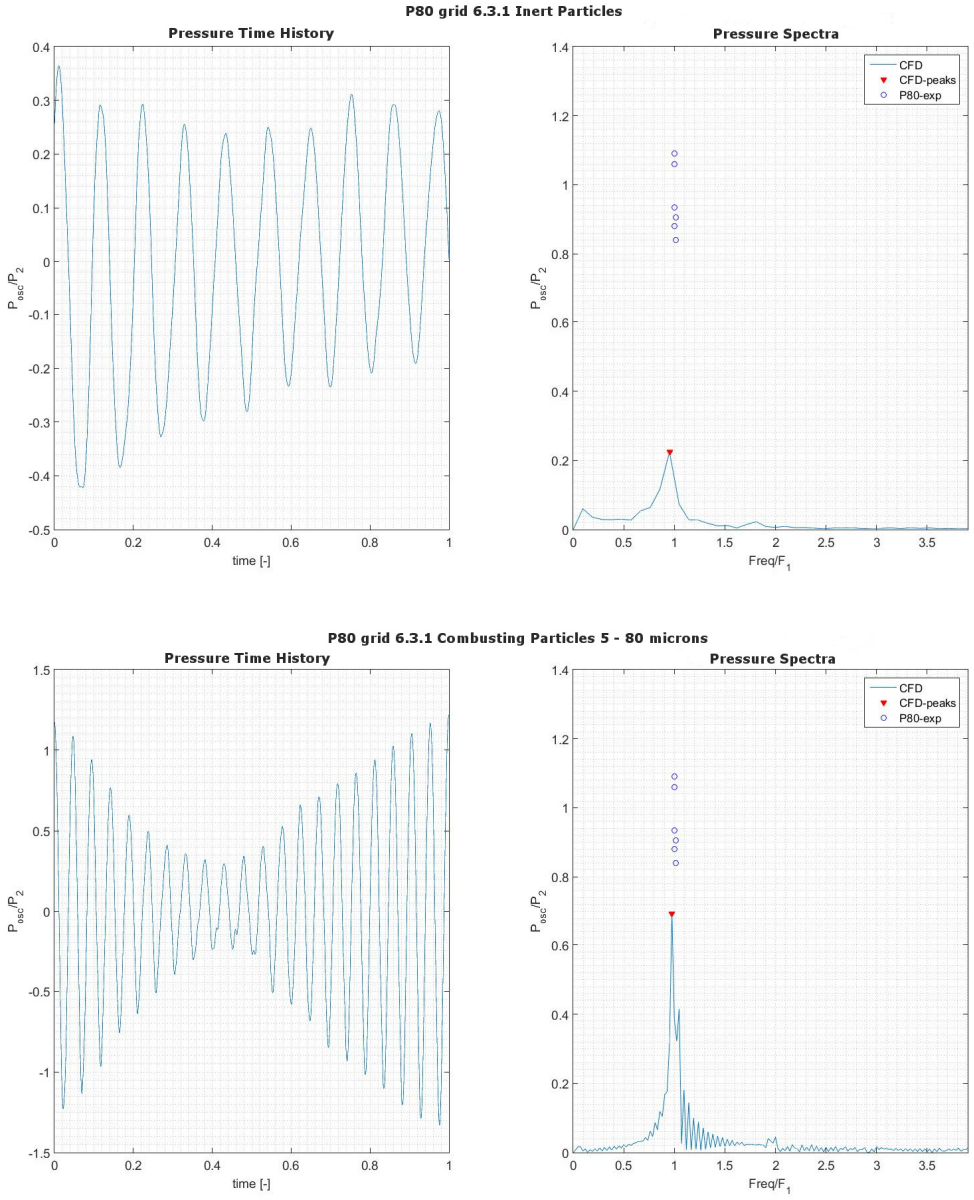

Figure 19 : P80 - Fourier Analysis of chamber pressure oscillations with inert (top) and combusting particles (bottom)

Fourier Analyses of pressure oscillations showing details of frequencies and amplitudes for the two cases of inert particles and combusting particles are shown in Figure 19. With reacting particles the calculated instability frequency rises about 2% from that of the inert case and the oscillation amplitude rises by about 210%.

Comparison of the particle diameter distributions for the inert and reacting particle simulations is shown Figure 20 for the same statistical selection of particles (i.e. visualize 1 particle in every 25). It is evident that there is a coarser distribution of larger particles (red) in the inert case and the vortical structures are far less extended than in the case with reacting particles where a dense concentration of fine (blue) particles surrounds the main vortices.

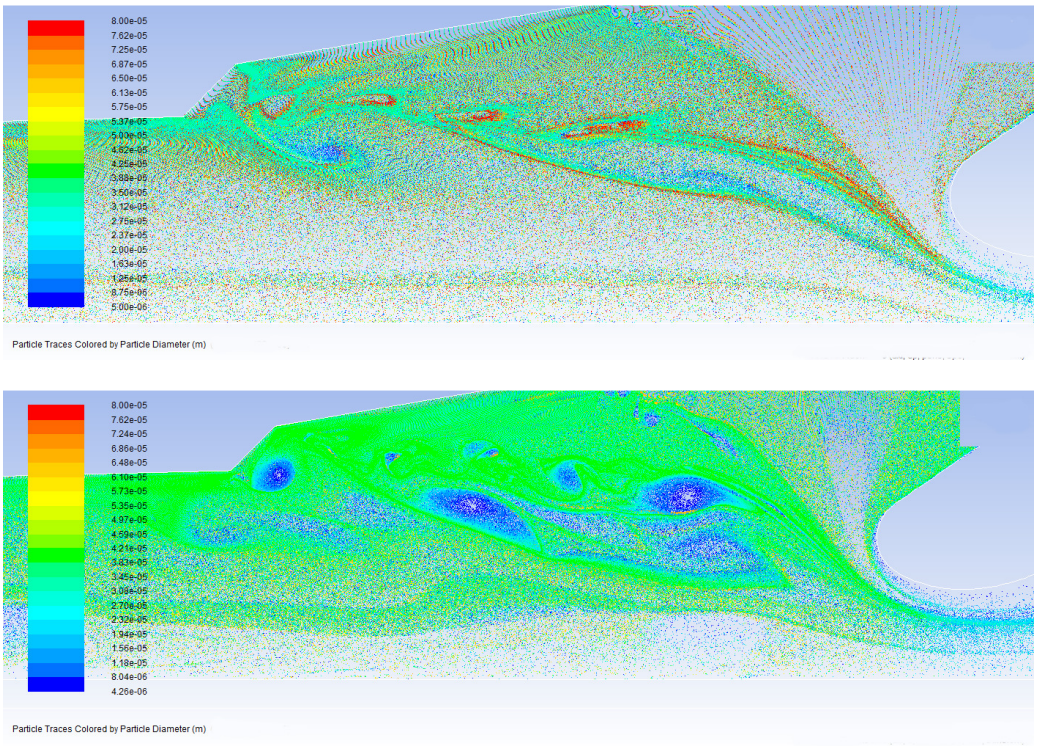

Figure 20 : P80 - Comparison of particle diameters, inert (top), reacting (bottom)

A potential explanation for the above phenomena is that in the case of reacting particles there is a much greater proportion of finer particles associated with the oxide residues than in the inert case. Additionally the energy within the flow is higher and consequently the energy contained within the vortices is higher. The finer particles are more easily convected to the outer regions of the vortices where particle packs are more easily created. Mass transfer of a reduced number of large particles to the vortices takes place but the damping is diminished since there are fewer larger particles and the vortices themselves contain more energy. Additionally there may be some energy transfer between the vortices.

As a consequence, for the case with reacting particles, the vortices crossing the cavity entrance are more well-defined and reinforce the upstream acoustic wave feedback phenomena. Additionally the particle concentrations between vortices are greater and have greater masses leading to a disturbance of the sonic line with an associated pressure peak thereby enforcing the pressure oscillations as discussed previously by Guery-et-al[15].

V. Concluding Remarks

The aim of the present work was to, firstly, confirm the validity of methodology developed to simulate two phase flow containing combusting aluminium particles originating from an AP/HTPB propellant in a real solid rocket motor configuration in which combustion instabilities have been identified.

Two validation test cases have been identified, the ONERA C1 rocket motor for which theoretical results are available and the C1xb rocket motor for which experimental results are available.

The investigation concluded with application of the method developed to the P80 SRM for which experimental results in term of chamber pressure, pressure amplitudes and instability frequencies are available.

The activity involved the application of the Discrete Phase Model in FLUENT 15 to model two phase flow using an Euler-Lagrange coupling mechanism to link the gas and particle phases and included a customized User Defined Function (UDF) to account for details of aluminium particle combustion processes. Axisymmetric calculations were performed.

For the ONERA C1 validation test case good quantitative and qualitative agreement was obtained between the present method and results from similar computations by Najjar-et-al[2].

For the C1xb validation test case, using inert alumina particles, very good quantitative agreement was obtained between the results from the present method and experiment. Results using this method for the purely hydrodynamic test case compared less favorably with experiment but were, however, better than results from other investigators cited in the literature.

A possible explanation for this is that calculations using the droplet model yield a significantly greater contribution to the pressure amplitudes in the simulation and override the inclusion or exclusion of any 3D mean flow effects which may be responsible for the discrepancies with experiment when particles are absent.

For the P80 test case the critical parameters in the first part of the investigation were the importance of creating suitable grids upon which to perform such calculations for the hydrodynamic test case. If the grids are too coarse the details of vortices are lost, if they are too fine, the vortices become damped due to too much numerical dissipation.

The results for the hydrodynamic case show that when using a customized finer grid in the region of the igniter, the same regular level of oscillations as those present on the finest grid are obtained. Four sources of vortex shedding are present, three associated with CVS locations and one associated with PVS.

Additionally, for the hydrodynamic case there is good agreement with experiment for the computed instability frequency on all grids whereas only the amplitudes of the pressure oscillations on the finest grid are in best agreement with experiment. It is hypothesized that the large aft cavity may be responsible for a significant contribution to the instabilities due the generation of sound waves as the vortices travel almost normally across the cavity entrance

The second part of the P80 investigation attempted to isolate critical features which were responsible for different levels of instability by comparing results between inert and combusting particles. Again, two kinds of vortex shedding were identified, corner vortex shedding and parietal vortex shedding which were both affected by the size of the particles in their vicinity. Fundamental to the correct simulation of vortices and the associated pressure oscillations was the selection of the correct injection particle distribution and range of particle sizes. Since the majority of the combustion process occurs in the vicinity of the propellant grain surface where both parietal vortex shedding and corner vortex shedding originate, an injection particle size which is too large serves to dampen the vortices which are in the combustion zone thereby reducing the level of pressure oscillations.

An attempt has also been made to explain the mechanism(s) for pressure oscillations in these kind of SRM configurations following ideas which have been suggested in the literature. Such mechanisms are subject to verification.

The results from the present study for the P80 test case indicate that the instabilities in the hydrodynamic computation (gas only – no particles) are greater than the instabilities with combusting particles where the amplitudes of pressure oscillations are about 85% higher than in the combusting particle computation.

Additionally, the correct selection of particle size and range in the particle distribution along the injection surface is fundamental to the satisfactory modelling of pressure oscillation amplitudes in the combusting particle simulations.

Acknowledgements

This work is funded and supported by the AVIO S.p.A./VECEP Programme under Project VEGA C3 (phase C – 2016). The original UDF software and experimental data have been kindly supplied by AVIO S.p.A.

References

1. ANSYS FLUENT 12.0 Theory Guide, 7.4-7.6, Fluent Inc., Canonsburg, Pennsylvania, USA, 2009.

2. Najjar, F.M., Ferry, J.P., Hasaelbacher, A., and Balachandar, S., "Simulations of Solid-Propellant Rockets: Effects of Aluminium Droplet Size Distribution", Journal of Spacecraft and Rockets, Vol. 43, No. 6, 2006, pp 1258-1270.

3. Dupays, J., Prevost, M., Tarrin, P., and Vuillot, F., "Effects of particulate phase on vortex shedding driven oscillations in solid rocket motors2, 32nd AIAA/ASME/SAER/ASEE Joint Propulsion Conference, Lake Buena Vista, FL.

4. Boris, J.P., Grinstein, F.F., Oran, E.S., and Kolbe, R.J.,"New Insights into Large Eddy Simulation," Fluid Dynamics Research, Vol. 10, No. 4-6, 1992, pp. 199-227.

5. Lupoglazoff, N. and Vuillot, F. "Numerical Simulation of Vortex Shedding Phenomenon in 2D Test Case Solid Rocket Motors", AIAA Paper 92-0776, 30th Aerospace Sciences Meeting & Exhibit, Reno, NV, January 1992.

6. Beckstead, M.W. "A Summary of Aluminium Combustion", RTO-EN-23.

7. Widener, J. F.,Beckstead, M. W., "Aluminium Combustion Modelling in Solid Propellant Combustion Products", AIAA-98-3824.

8. Zhao,H.,Liu,H.F., Xu,J.L., Li,W. F., Lin, K.F., "Temporal properties of secondary drop breakup in the bag-stamen breakup regime", Physics of Fluids ,Vol. 25, 2013.

9. Kourta, A., "Computation of Vortex Shedding in Solid Rocket Motors Using Time-Dependent Turbulence Model", J. Propulsion & Power, Vol. 15, No. 3, pp 390-400, 1999.

10. Paglia F., "Private Communication"AVIO, Colleferro, Italy, 2016.

11. Gallier, S., Prevost, M., Hijlkema, J. and Roumy, M., "Effects of Cavity on Thrust Oscillations in Subscale Solid Rocket Motors", 45th AIAA/ASME/SAE/ASEE Joint Propulsion Conference &Exhbit, 2-5 August, 2009, Denver, Colorado, AIAA 2009-5253.

12. Anthoine, J.,Buchlin,J.M and Guery, J.F., "Experimental and Numerical Investigations of Nozzle Geometry effect on the Instabilities in Solid Propellant Boosters",AIAA Paper 2000-3560, July 2000.

13. Anthoine, J., and Lema, M., "Passive Control of Pressure Oscillations in Solid Rocket Motors : Cold Flow Experiments", J. Prop. Power, 25 (3), 2009.

14. Howe, M. "The dissipation of Sound at an Edge",J. Sound. Vib., 70, 1980.

15. Guery, J.F., Ballereau, S., Godfroy, F., Gallier, S., Orlandi, O., Della Pietra, P.,"Thrust Oscillations in Solid Rocket Motors", 44th AIAA/ASME/SAE/ASEE Joint Propulsion Conference & Exhibit, 21-23 July 2008, Hartford, CT. AIAA-2008-4979.